AIAA JOURNAL
Vol. 33, No. 10, October 1995

Computational Model of Flexible Membrane Wings in Steady Laminar Flow

Richard Smith* and Wei Shyy†
University of Florida, Gainesville, Florida 32611

A computational procedure is presented that models the interaction of a two-dimensional flexible membrane wing and laminar, high-Reynolds-number fluid flow. The membrane wing model is derived by combining a spatial-coordinate-based finite difference formulation of the equilibrium statement for an elastic membrane with a pressure-based control volume formulation of the incompressible Navier–Stokes equations written in general curvilinear body-fitted coordinates. The model is applied to initially flat membrane wings of both vanishing and finite material stiffness as well as to flexible inextensible wings with excess length. Computational results are presented for Reynolds numbers between 2×10^3 and 10^4. The results from the viscous-flow-based membrane wing model are compared with predictions using a potential-flow-based model as well as with experimental data for membrane wings in turbulent flow. Although the assumption of laminar flow precludes a quantitative comparison with the available experimental data, the solutions obtained capture many of the significant features of the aeroelastic interaction that are unaccounted for with a potential flow description of the fluid dynamics.

Nomenclature

A	= coefficient in difference equation
A_{ij}	= aerodynamic influence coefficients
C_D	= drag coefficient
C_L	= lift coefficient
C_M	= quarter-chord moment coefficient
C_P	= pressure coefficient
C_T	= tension coefficient
c	= membrane chord length
E	= Young's modulus of membrane material
h	= membrane thickness
J	= Jacobian of the transformation
L	= membrane length
L_0	= initial membrane length
n_i	= Cartesian component of unit normal
p	= flowfield pressure
q_1, q_2, q_3	= geometric quantities
q_∞	= freestream stagnation pressure
Rn	= Reynolds number
S	= source term in difference equation
${}^0S$	= stress in prestrained configuration
T	= membrane tension
V_i	= contravariant component of velocity
v_i	= Cartesian component of fluid velocity
x_i	= Cartesian coordinates
α	= angle of attack
Γ_j	= point vortex strengths
Δp	= pressure jump across membrane
δ	= membrane strain
ε	= excess length parameter
μ	= fluid viscosity
ξ_i	= curvilinear coordinates
τ	= fluid shear stress at membrane
Π_1, Π_2	= inviscid aeroelastic parameters
ϱ	= fluid density

Subscripts

E, W	= grid points adjacent to point P
i, j	= partial derivative of component i with respect to j
∞	= freestream value

Superscripts

$+, -$	= values at upper and lower surfaces of membrane
$'$	= perturbation

Introduction

THE vast majority of the published works related to membrane wing aerodynamics have made several simplifying approximations concerning both the elastic characteristics of the membrane itself as well as the nature of the surrounding flowfield. Perhaps the most significant of these simplifying assumptions is that the fluid dynamics can be adequately described by a potential based model of the flowfield. In addition to the almost universally adopted potential flow assumption, the additional approximations associated with thin airfoil theory—small camber and incidence angle—are also often made, and the membrane itself is generally considered to be inextensible. The purpose of this work is to present a model that fully accounts for the effects of viscosity in the fluid and to investigate the aerodynamics of membrane wings near the upper limit of the laminar flow regime.

The analysis of membrane wings begins with the historical works of Voelz,[1] Thwaites,[2] and Nielsen.[3] These works considered the steady, two-dimensional, irrotational flow over an inextensible membrane with slack. As a consequence of the inextensible assumption and the additional assumption of small camber and incidence angle, the membrane wing boundary value problem is linearized and may be expressed compactly in nondimensional integral equation form as

$$1 - \frac{C_T}{2} \int_0^1 \frac{[\mathrm{d}^2(y/a)/\mathrm{d}\zeta^2]}{2\pi(\zeta - x)}\,\mathrm{d}\zeta = \frac{\mathrm{d}(y/\alpha)}{\mathrm{d}x} \tag{1}$$

where $y(x)$ defines the membrane profile as a function the x coordinate, and α is the flow incidence angle. Equation (1) has been referred to as the "Thwaites sail equation" by Chambers[4] and simply as the "sail equation" by Newman[5] and Greenhalgh et al.[6] This equation, together with a dimensionless geometric parameter ε that specifies the excess length of the membrane, completely defines the linearized theory of an inextensible membrane wing in a steady, inviscid flowfield.

Received March 10, 1994; revision received Jan. 21, 1995; accepted for publication Jan. 21, 1995.

*Postdoctoral Associate, Department of Engineering, Mechanics, and Engineering Science. Member AIAA.

†Professor, Department of Engineering, Mechanics, and Engineering Science. Associate Fellow AIAA.

Different analytic and numerical procedures have been applied to the sail equation to determine the membrane shape, aerodynamic properties, and membrane tension in terms of the angle of attack and excess length. In particular, Thwaites[2] obtained eigensolutions of the sail equation that are associated with a wing at the ideal (singularity free) angle of incidence. Nielsen[3] obtained solutions to the same equation using a Fourier series approach that is valid for wings at angles of incidence other than the ideal angle. Other more recent but similar works are those by Vanden-Broeck and Keller,[7] Greenhalgh et al.,[6] and Sugimoto and Sato.[8]

Various extensions of the linear theory have appeared in the literature over the years. Vanden-Broeck[9] as well as Murai and Maruyama[10] developed nonlinear theories valid for large camber and incidence angle. The effect of elasticity has been included in the membrane wing theories of Jackson[11] and Sneyd,[12] and the effects of membrane porosity have been investigated by Murata and Tanaka.[13] In a paper by de Matteis and de Socio,[14] experimentally determined separation points were used to modify the lifting potential flow problem in an attempt to model flow separation near the trailing edge. The effects of elasticity and porosity were also considered in this work. A comprehensive review of the work published before 1987 related to membrane wing aerodynamics is given by Newman.[5]

Comparisons of the various potential flow based membrane wing theories with experimental data have been reported by several authors including Greenhalgh et al.,[6] Sugimoto and Sato,[8] and Newman and Low.[15] In general, there has been considerable discrepancy between the measurements made by the different authors, which have all been in the turbulent flow regime at Reynolds numbers between 10^5 and 10^6. As a result of the discrepancies in the reported data—primarily due to differences in Reynolds number and experimental procedure—the agreement between the potential based membrane wing theories and the data has been mixed.[16] Flow visualization studies indicate the main reason for the disagreement is the existence of a thick boundary layer or region of separated flow on the membrane, typically near the trailing edge. It has been noted by several authors that the presence of viscous effects such as thick boundary layers and separation regions will overshadow any implications associated with the linearizing approximations made by thin wing theory.[5]

Governing Equations

Membrane Equilibrium

In this section the general equilibrium equations are presented for a two-dimensional elastic membrane subjected to both normal and shearing stresses. The membrane is assumed to be massless and the equilibrium conditions are stated in terms of the instantaneous spatial Cartesian coordinates x_i and the body-fitted curvilinear coordinates ξ_i. The basic formulation is essentially identical to many previously published works such as de Matteis and de Socio[14] and Sneyd.[12]

Figure 1 illustrates an elastic membrane restrained at the leading and trailing edges subjected to both fluid dynamic pressure and shear stress, p and τ, respectively. Imposing equilibrium in the normal and tangential directions requires

$$\frac{d^2x_2}{dx_1^2}\left(1+\frac{dx_2}{dx_1}\right)^{-\frac{3}{2}} = -\left(\frac{\Delta p}{T}\right) \tag{2}$$

$$\frac{dT}{d\xi_1} = -\tau \tag{3}$$

Equation (2) is often referred to as the Young–Laplace equation.[17] The net pressure and shear stress acting on a segment of the membrane are given, respectively, by

$$\Delta p = p^- - p^+ \tag{4}$$

$$\tau = \tau^- + \tau^+ \tag{5}$$

where the superscript indicates the value at the upper and lower surface of the membrane as shown in the figure. In the membrane material is assumed to be linearly elastic, the nominal membrane

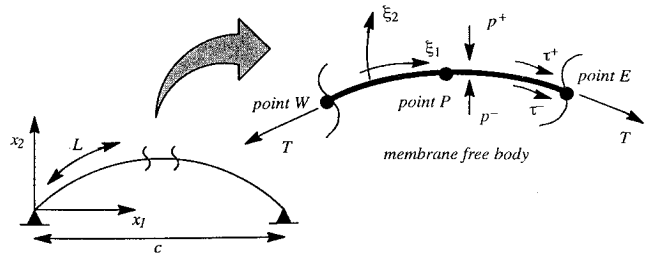

Fig. 1 End constrained elastic membrane.

tension $\bar{T}$ may be written in terms of the nominal membrane strain $\bar{\delta}$ as

$$\bar{T} = ({}^0S + E\bar{\delta})h \tag{6}$$

The nominal membrane strain is given by

$$\bar{\delta} = (L - L_0)/L_0 \tag{7}$$

where L_0 is the prestrained length of the membrane and L is the length of the membrane after deformation, which may be expressed in terms of the spatial coordinates x_i as

$$L = \int_0^c \sqrt{1+\left(\frac{dx_2}{dx_1}\right)^2}\,dx_1 \tag{8}$$

At the leading and trailing edges of the membrane the following boundary conditions are imposed on Eq. (2):

$$x_2 = 0 \quad \text{at} \quad x_1 = 0, c \tag{9}$$

Fluid Dynamic Conservation Laws

The governing conservation laws for steady, laminar, incompressible flow are the Navier–Stokes equations, which may be written in two-dimensional Cartesian coordinates as

$$\frac{\partial}{\partial x_j}(\varrho v_j v_1) = \frac{\partial}{\partial x_j}(\mu v_{1,j}) - \frac{\partial p}{\partial x_1} \tag{10}$$

$$\frac{\partial}{\partial x_j}(\varrho v_j v_2) = \frac{\partial}{\partial x_j}(\mu v_{2,j}) - \frac{\partial p}{\partial x_2} \tag{11}$$

$$\frac{\partial}{\partial x_j}(\varrho v_j) = 0 \tag{12}$$

When new independent variables ξ_1 and ξ_2 are introduced, Eqs. (10–12) change according to the general transformation $\xi_1 = \xi_1(x_1, x_2, t)$ and $\xi_2 = \xi_2(x_1, x_2, t)$. Equations (10–12) can be rewritten as follows, where the subscript i, j indicates the partial derivative of the i Cartesian component of velocity or position with respect to the curvilinear coordinate j:

$$\frac{\partial}{\partial \xi_j}(\varrho V_j v_1) = \frac{\partial}{\partial \xi_1}\left[\frac{\mu}{J}(q_1 v_{1,1} - q_2 v_{1,2})\right] + \frac{\partial}{\partial \xi_2}\left[\frac{\mu}{J}(q_3 v_{1,2} - q_2 v_{1,1})\right] - \frac{\partial}{\partial \xi_1}(x_{2,2}p) + \frac{\partial}{\partial \xi_2}(x_{2,1}p) \tag{13}$$

$$\frac{\partial}{\partial \xi_j}(\varrho V_j v_2) = \frac{\partial}{\partial \xi_1}\left[\frac{\mu}{J}(q_1 v_{2,1} - q_2 v_{2,2})\right] + \frac{\partial}{\partial \xi_2}\left[\frac{\mu}{J}(q_3 v_{2,2} - q_2 v_{2,1})\right] + \frac{\partial}{\partial \xi_1}(x_{1,2}p) + \frac{\partial}{\partial \xi_2}(x_{1,1}p) \tag{14}$$

$$\frac{\partial}{\partial \xi_j}(\varrho V_j) = 0 \tag{15}$$

where the contravariant velocity components are given by

$$V_1 = (v_1)x_{2,2} - (v_2)x_{1,2} \tag{16}$$

$$V_2 = (v_2)x_{1,1} - (v_1)x_{2,1} \tag{17}$$

and

$$q_1 = (x_{1,2})^2 + (x_{2,2})^2 \tag{18}$$

$$q_2 = x_{1,1}x_{1,2} + x_{2,1}x_{2,2} \tag{19}$$

$$q_3 = (x_{1,1})^2 + (x_{2,1})^2 \tag{20}$$

and the Jacobian of the transformation is defined as

$$J = x_{1,1}x_{2,2} - x_{1,2}x_{2,1} \tag{21}$$

The following nonslip boundary condition is imposed on the Cartesian components of the fluid velocity vector at the membrane surface

$$v_i = 0 \tag{22}$$

and the fluid velocity far upstream of the membrane is given by

$$v_1 = v_\infty \cos\alpha \tag{23}$$

$$v_2 = v_\infty \sin\alpha \tag{24}$$

where v_∞ is the freestream velocity.

Nondimensionalization of the Governing Equations

The aeroelastic boundary value problem can be written in nondimensional form after introducing appropriate dimensionless variables. Substituting these variables into Eq. (2) leads to the following dimensionless equilibrium equation:

$$\frac{d^2x_2}{dx_1^2}\left(1 + \frac{dx_2}{dx_1}\right)^{-\frac{3}{2}} = -\left(\frac{1}{\Pi_1}\right)^3 \frac{\Delta p}{T} \tag{25}$$

when membrane tension is dominated by elastic strain, with Π_1 defined to be

$$\Pi_1 = (Eh/q_\infty c)^{\frac{1}{3}} \tag{26}$$

or

$$\frac{d^2x_2}{dx_1^2}\left(1 + \frac{dx_2}{dx_1}\right)^{-\frac{3}{2}} = -\left(\frac{1}{\Pi_2}\right) \frac{\Delta p}{T} \tag{27}$$

when membrane tension is dominated by pretension, with Π_2 defined to be

$$\Pi_2 = \left({}^0Sh/q_\infty c\right) \tag{28}$$

where q_∞ is the freestream stagnation pressure equal to $\frac{1}{2}\varrho v_\infty^2$. The use of the cube root in the definition of Π_1 in Eq. (26) is suggested by the exact solution of Eq. (2) given by Seide.[18]

The physical significance of the aeroelastic parameters Π_1 and Π_2 is that the nondimensional deformation of an initially flat, elastic membrane is inversely proportional to Π_1 in the absence of pretension. Alternatively, the deformation of a membrane is inversely proportional to Π_2 in the presence of large initial pretension. Consequently, the steady-state, inviscid, aeroelastic response of an initially flat membrane wing at a specified angle of attack is controlled exclusively by Π_1 in the limit of vanishing pretension and exclusively by Π_2 in the limit of vanishing material stiffness.

Substituting the same dimensionless variables into Eqs. (10–12) leads to the following nondimensional form of the incompressible Navier–Stokes equations:

$$\frac{\partial}{\partial x_j}(v_j v_1) = \left(\frac{1}{Rn}\right)\frac{\partial}{\partial x_j}(v_{1,j}) - \frac{\partial p}{\partial x_1} \tag{29}$$

$$\frac{\partial}{\partial x_j}(v_j v_2) = \left(\frac{1}{Rn}\right)\frac{\partial}{\partial x_j}(v_{2,j}) - \frac{\partial p}{\partial x_2} \tag{30}$$

$$\frac{\partial}{\partial x_j}(\varrho v_j) = 0 \tag{31}$$

The dimensionless parameter appearing in Eq. (29) and Eq. (30), the Reynolds number, is defined as

$$Rn = v_\infty \varrho c/\mu \tag{32}$$

If the membrane is not initially taut, the geometry of the wing may be characterized by an additional dimensionless quantity, the excess length ε, defined as follows:

$$\varepsilon = (L_0 - c)/c \tag{33}$$

The set of dimensionless parameters given above—Π_1, Π_2, Rn, ε, and α—completely characterize the physical problem considered in the present work.

Numerical Method

Membrane Equilibrium

A discrete form of the elastic membrane boundary value problem can be obtained at a finite number of points on the fixed interval $[0, c]$ by replacing the derivatives in Eq. (2) and the integral in Eq. (8) with appropriate finite difference and finite sum approximations. Applying central difference approximations to Eq. (2) leads to a three point difference kernel centered around point P with neighboring points E and W as shown in Fig. 1. At each point P an equation of the general form

$$A_p x_{2_p} = A_E x_{2_E} + A_W x_{2_W} + S_{x_2} \tag{34}$$

is then obtained where the various A are coefficients associated with the finite difference approximation, and S_{x2} is a source term containing all terms in Eq. (2) that cannot be expressed as a linear combination of the x_2 coordinates. Consequently, all of the nonlinearity in the elastic boundary value problem is contained in the source term.

Fluid Dynamic Conservation Laws

A pressure-based numerical procedure originally proposed by Patankar and Spalding[19] for Cartesian coordinates was chosen for computing the laminar, incompressible flow surrounding a two-dimensional wing of vanishing thickness in an unbounded domain. The details of the basic pressure correction algorithm are given in Patankar[20] with the extension of the procedure to general curvilinear coordinates given in Shyy.[17] The present implementation of the algorithm follows the work of Braaten and Shyy[21] with the second-order upwind scheme of Shyy et al.[22] adopted for the convection terms in the momentum equations. Details of the pressure-based solution algorithm may be found in the references and will not be repeated here.

Aeroelastic Computational Procedure

The primary objective of the present work is to determine the equilibrium configuration and associated aerodynamic characteristics of an elastic membrane wing in a viscous fluid. Consequently, the present task consists of finding membrane configurations and aerodynamic surface pressures and shear stresses that simultaneously satisfy Eq. (2) and Eqs. (13–15), respectively. An iterative procedure is used to solve the coupled boundary value problem by computing the elastic and aerodynamic problems cyclically until a solution is obtained that satisfies the governing equations to a predetermined convergence criterion.

During the course of the aeroelastic iteration procedure, it is necessary to update the grid in the physical domain so that it remains body fitted as the wing deforms. The maintenance of the body-fitted grid is achieved by updating the grid points in the vicinity of the membrane during the course of iteration according to the following formula:

$$x_2^{(i)} = x_2^{(i-1)} + g(\xi_2)\left[x_2^{(i)} - x_2^{(i-1)}\right] \tag{35}$$

where $g(\xi_2)$ is a general function that decays with distance away from the membrane surface. The superscripts appearing in Eq. (35)

indicate the level of the aeroelastic iteration procedure. Currently, $g(\xi_2)$ is chosen as an exponential function defined as

$$g(\xi_2) = \exp(-|\xi_2|/c_1) \tag{36}$$

where c_1 is a constant that depends on the grid resolution and the Reynolds number. A similar strategy using an exponentially decaying function for updating field grid points while maintaining a body-fitted curvilinear grid has been used by Boschitsch and Quackenbush.[23]

Potential Flow Model for Thin Wings

In this section a method is presented for computing the surface pressure distribution resulting from the irrotational, incompressible flow over thin, two-dimensional wings of arbitrary shape. The reason for including in the present work a numerical procedure for the solution of lifting potential flows is to highlight the difference in aerodynamic quantities predicted by a viscous flow based membrane wing model when compared with previous work on membrane wing aerodynamics based on a potential description of the flowfield. The use of point vortex singularities to model the lifting potential flow around thin wings has its historical origin and justification in work by James.[24] A description of the method in its modern form may be found in Katz and Plotkin.[25]

By modeling the wing as an assemblage of vortex singularity segments of unknown strength and enforcing the zero normal relative velocity condition at each control point, designated as point i, the following set of linear algebraic equations may be formed and solved for the vortex strength Γ at point j:

$$A_{ij}\Gamma_j = (-\boldsymbol{v}_\infty \cdot \boldsymbol{n})_i \tag{37}$$

In Eq. (37) A_{ij} is a matrix of vortex influence coefficients, defined as the normal velocity induced at control point i by a unit strength vortex at point j, and $\boldsymbol{n}$ is the unit normal vector at the control point.

Once the vortex strengths have been determined from Eq. (37), the perturbation velocities on the upper and lower surfaces, $\boldsymbol{v}'^{+}$ and $\boldsymbol{v}'^{-}$, respectively, are given by

$$\boldsymbol{v}'^{+} = \frac{\Gamma}{2l}\begin{bmatrix} n_2 \\ -n_1 \end{bmatrix} \tag{38}$$

$$\boldsymbol{v}'^{-} = \frac{\Gamma}{2l}\begin{bmatrix} n_2 \\ -n_1 \end{bmatrix} \tag{39}$$

where l is the length of the segment.

With the velocity field determined on the upper and lower surface of the wing, the pressure on the wing surfaces, p^+ and p^-, may be computed directly from the Bernoulli equation as follows:

$$p^{\pm} = \tfrac{1}{2}\varrho\left(v_\infty^2 - v^{\pm 2}\right) + p_\infty \tag{40}$$

It should be pointed out that the leading-edge suction force arising from the pressure singularity at the leading edge of the infinitely thin membrane is not included in the preceding potential flow model.

Test Cases

Elastic Membrane Under a Uniform Pressure Load

For this test case the pretension is chosen to be zero; consequently, the elastic response of the membrane is completely described by the nondimensional stiffness parameter Π_1. As the inextensible limit is approached and Π_1 tends to infinity, the geometric nonlinearity intrinsic in the problem becomes more pronounced, and the elastic boundary value problem becomes algorithmically stiff. Consequently, the use of underrelaxation becomes essential to ensure convergence of the numerical scheme. This is significant since most of the practical applications for membrane wings, as well as the available experimental data, are for flexible but nearly inextensible membranes.

Figure 2 shows a comparison of the computed midpoint coordinate of the membrane with an analytic solution for an elastic membrane given by Seide.[18] Here, uniform pressure has been substituted for the stagnation pressure in the definition of Π_1. The computed solutions and the analytic results are essentially indistinguishable.

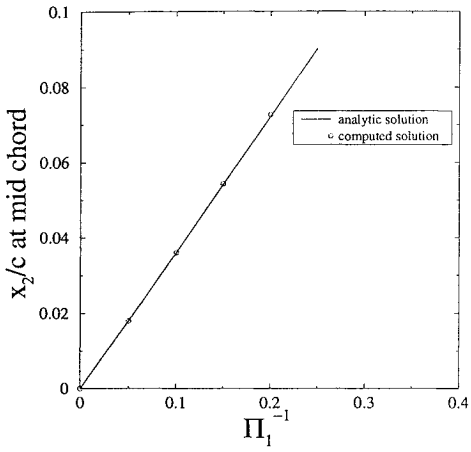

Fig. 2 Computed midchord coordinate for an initially flat, uniformly loaded elastic membrane.

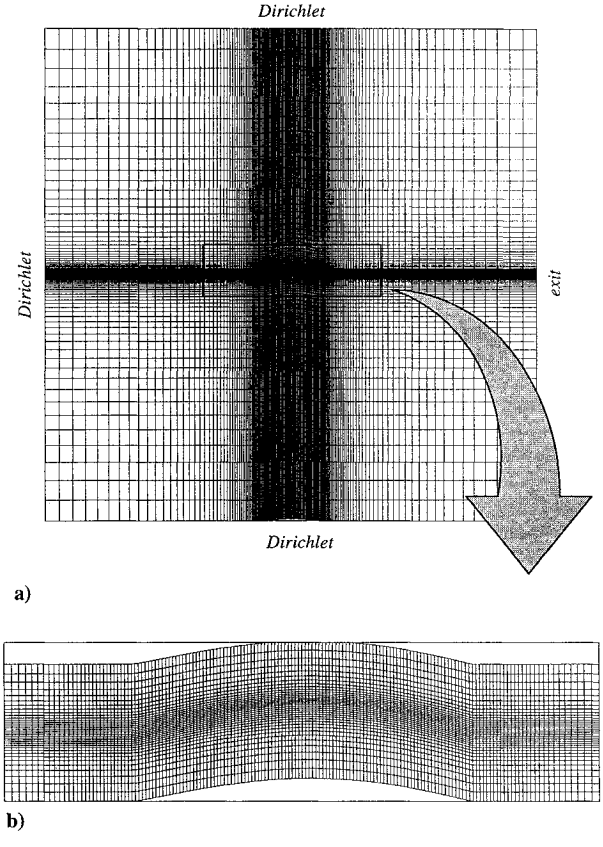

Fig. 3 Typical grid used for membrane wing computations: a) complete computational domain and boundary conditions and b) enlarged view of the grid near the membrane.

Effect of Outer Boundary Location

Since the physical problem under consideration is the flow over a wing in an unbounded domain, the placement and boundary conditions imposed on the outer boundary of the computational domain require investigation. Consequently, a sequence of computations was performed to assess the sensitivity of the computed results to the location and the boundary conditions imposed at the outer flow boundary.

Figure 3 shows a typical grid used in the membrane wing computations. The wing is situated in the center of a square computational domain typically $10c \times 10c$ in size. The freestream velocity is imposed on all outer flow boundaries except the downstream boundary where a zero gradient condition is imposed on the velocity

Table 1 Effect of outer boundary location on computed aerodynamic properties of a rigid, 2% camber, zero thickness, circular arc airfoil at $\alpha = 5$ deg and $Rn = 4 \times 10^3$

Grid	Domain size	C_L	C_D	C_M
185 × 77	$5c \times 5c$	0.637	0.0761	0.0442
207 × 91	$10c \times 10c$	0.626	0.0752	0.0425
221 × 101	$15c \times 15c$	0.623	0.0750	0.0422
247 × 121	$30c \times 30c$	0.621	0.0749	0.0420

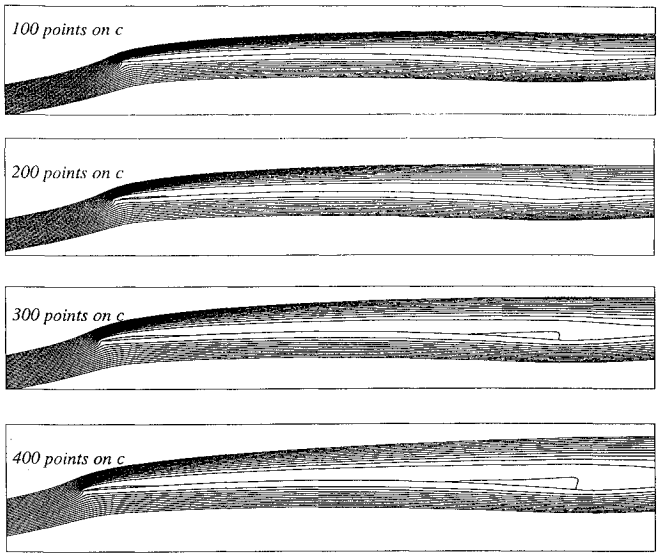

Fig. 4 Effect of grid refinement on stream function contours for a rigid, 2% camber, zero thickness, circular arc airfoil at $\alpha = 5$ deg and $Rn = 4 \times 10^3$.

components. An enlarged view of the grid in the vicinity of the wing is also shown in the figure.

The effect of moving the outer boundary away from a rigid, zero thickness circular arc airfoil may be seen in Table 1. The boundary was moved outward by adding additional grid points to the basic $5c \times 5c$ grid so that the outer boundary location is isolated from other grid dependency issues. As may be seen from the table, there is very little change—less than 1%—in the computed lift, drag, and aerodynamic moment beyond a domain size of $10c \times 10c$. Consequently, a computational domain size of $10c \times 10c$ with exit conditions imposed at the downstream boundary is adopted for all further computations.

Effect of Grid Refinement

The principal test case for investigating the effect of grid refinement on the computed flowfield is a rigid, 2% camber, zero thickness, circular arc airfoil at 5 deg angle of attack and a Reynolds number of 4×10^3. Figure 4 shows the computed streamlines for the circular arc airfoil using 100, 200, 300, and 400 grid points along the wing chord. The most significant flow feature to emerge as the grid is refined is the recirculation region near the trailing edge and the attendant departure of the streamlines from the upper surface of the airfoil. The wake behind the airfoil may also be seen to thicken significantly with the appearance of the trailing-edge separation region. Based on the grid refinement sequence shown in Fig. 4, it may be concluded that for circular arc configurations—associated with either flexible or rigid wings—potential flow will not be capable of accurately describing the flowfield.

The computed lift, drag, and aerodynamic moment for the circular arc airfoil are presented in Table 2 for the grid refinement sequence shown in Fig. 4. Even at the highest grid resolution there is a 5–10% change in computed values when compared with the previous grid. However, it is expected that a completely grid independent solution will be difficult to obtain for this problem since a stringent requirement is placed on grid resolution at this Reynolds number.

Table 2 Effect of grid refinement on computed aerodynamic properties of a rigid, 2% camber, zero thickness, circular arc airfoil at $\alpha = 5$ deg and $Rn = 4 \times 10^3$

Grid	Points on c	C_L	C_D	C_M
207 × 91	100	0.626	0.0752	0.0425
311 × 93	200	0.595	0.0654	0.0394
411 × 95	300	0.567	0.0603	0.0378
531 × 105	400	0.531	0.0558	0.0352

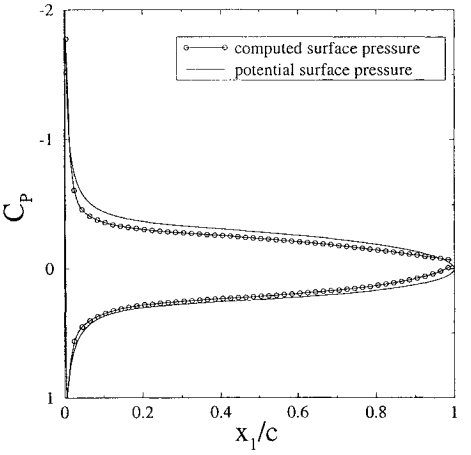

Fig. 5 Comparison of computed surface pressures at $Rn = 10^4$ and $\alpha = 3$ deg with potential flow solution for a rigid, zero thickness, 2% camber, circular arc airfoil; 100 grid points were used along the wing chord.

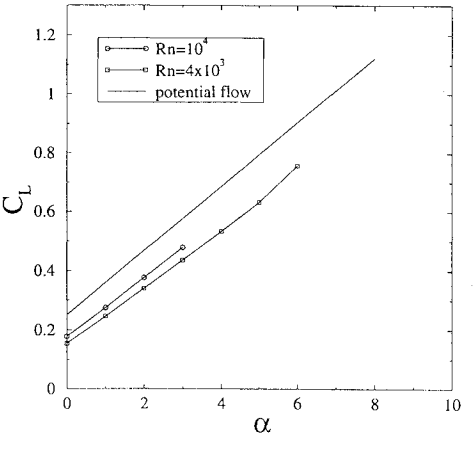

Fig. 6 Comparison of computed lift coefficient with potential flow solution for a rigid, zero thickness, 2% camber circular arc airfoil; 100 grid points were used along the wing chord.

Based on the results for a circular arc airfoil it may be expected that computations with a flexible membrane will exhibit a similar sensitivity to grid refinement since the equilibrium configuration for an end constrained membrane is quite similar to a circular arc and will likely exhibit the same type of trailing-edge separation.

Figure 5 shows the computed aerodynamic surface pressures at a Reynolds number of 10^4 for a rigid, 2% camber circular airfoil at 3-deg angle of attack. The potential flow solution for a circular arc airfoil taken from Katz and Plotkin[25] is shown in the figure for comparison. The computed surface pressures for the arc airfoil are in reasonable agreement with the potential flow solutions. Figure 6 shows the computed lift curves using 100 grid points along the wing chord at Reynolds numbers of 10^4 and 4×10^3 for the rigid, circular arc airfoil. Inspection of Figs. 4 and 6 indicates there is a general loss of circulation, compared with potential flow theory, around the airfoil due to viscous effects near the trailing edge.

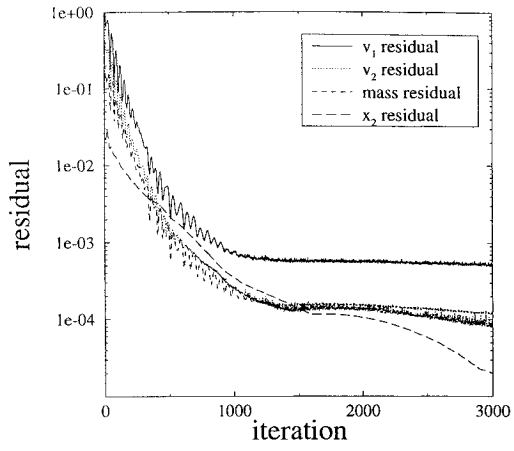

Fig. 7 Convergence path of the momentum, continuity, and equilibrium equations for an initially flat elastic membrane wing, $Rn = 4 \times 10^3$, $\alpha = 6$ deg, $\Pi_1 = 10$, $\Pi_2 = 0$, and $\varepsilon = 0$.

Aeroelastic Convergence Properties

Figure 7 illustrates the convergence path of the four coupled governing equations for an elastic membrane wing. It may be seen that the residuals are reduced to single precision machine accuracy after a few thousand iterations. Also, the terminal level of the residuals shown in the figure is consistent with the single precision floating point accuracy of the arithmetic used in the calculation. It may be noted that the stability of the aeroelastic algorithm is largely dictated by the choice of the relaxation parameter used in the solution of the membrane equilibrium equation.

Flexible Membrane Wing in a Viscous Fluid

Membrane wings may be broadly classified by considering the following three limiting cases of the parameters Π_1, Π_2, and ε. The first limiting case may be referred to as the elastic wing case with

$$\Pi_1 \sim \text{finite}$$
$$\Pi_2 = 0$$
$$\varepsilon = 0$$

In this case the wing is initially flat and taut but with no pretension. Consequently, the membrane behavior is determined exclusively by Π_1.

The second limiting case for membrane wings may be referred to as the constant tension wing case with

$$\Pi_1 = 0$$
$$\Pi_2 \sim \text{finite}$$
$$\varepsilon = 0$$

As with the first case the wing is initially flat and taut but now with sufficient pretension so that the material stiffness does not participate in determining the equilibrium membrane configuration.

The third limiting case may be referred to as the inextensible wing case with

$$\Pi_1 \sim \text{infinite}$$
$$\Pi_2 = 0$$
$$\varepsilon \sim \text{finite}$$

In this limiting case the wing is not initially flat and taut but has an excess length of material defined by the parameter ε. Of course, the Reynolds number and the angle of attack are additional parameters that characterize a steady flow about an airfoil, but they are to be distinguished from the three parameters listed earlier that characterize flexible membrane wing behavior.

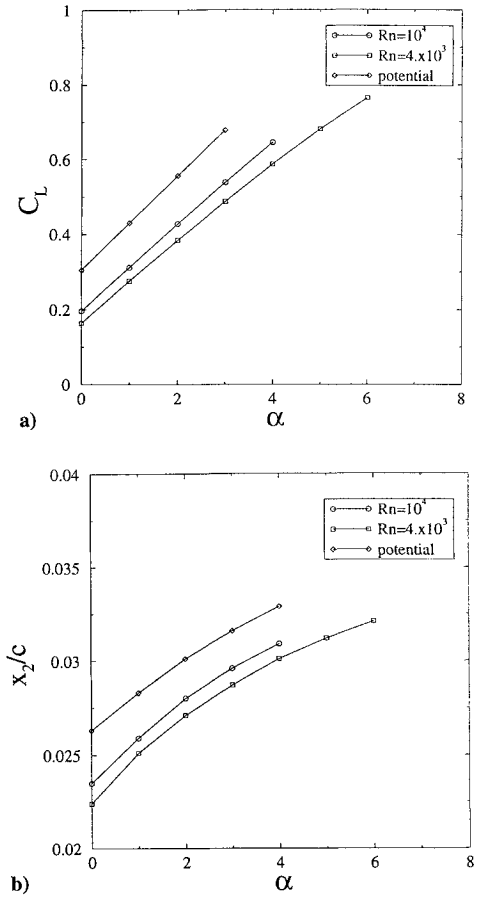

Fig. 8 a) Equilibrium lift coefficient and b) x_2 coordinate at midchord for an initially flat elastic membrane wing; $\Pi_1 = 10$, $\Pi_2 = 0$, and $\varepsilon = 0$; 100 grid points were used along the wing chord.

Elastic Membrane Case

Figure 8a shows the equilibrium lift coefficient for the first limiting case of an initially flat elastic membrane with $\Pi_1 = 10$, $\Pi_2 = 0$, and $\varepsilon = 0$. The figure shows the dependency on Reynolds number to be more pronounced for the elastic wing when compared with the rigid circular arc airfoil of Fig. 6. This may be explained by observing that the maximum wing camber, shown in Fig. 8b, follows the same trend as the lift coefficient. It may be concluded that this enhanced Reynolds number dependency is largely a result of the coupling between the membrane deformation and the flowfield. Also shown in the figure is the equilibrium lift coefficient predicted by a potential based membrane wing model for the same set of aeroelastic parameters. It may be seen that the potential based solution considerably overpredicts the lift on the wing even at small camber ratios and angles of attack when compared with the viscous flow based solution at these Reynolds numbers. The discrepancy between the potential solution and viscous flow solutions appears to be attributable to a general loss of circulation about the wing due to viscous effects primarily near the trailing edge.

Constant Tension Membrane Case

Figure 9a shows the equilibrium lift coefficient and maximum wing camber for the second limiting case of a constant tension membrane with $\Pi_1 = 0$, $\Pi_2 = 2$, and $\varepsilon = 0$. This figure may be contrasted with Fig. 8a. The contrast between constant tension and elastic wing characteristics may be reconciled by recalling that the response of an initially flat, constant tension membrane to a specified uniform pressure load is qualitatively different from the response of a membrane with finite material stiffness. For small deflections the constant tension membrane will respond linearly whereas an elastic membrane with finite material stiffness will exhibit a $\frac{1}{3}$ power law response to the applied pressure load[18] as shown in Fig. 2. A inspection of Figs. 8 and 9 illustrates the different behavior of the two membrane wings near 0 deg incidence. The initially flat,

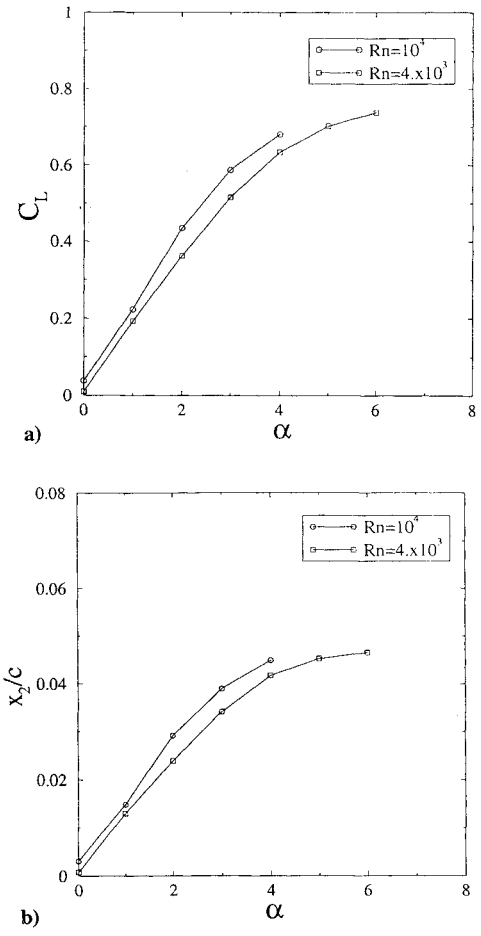

Fig. 9 a) Equilibrium lift coefficient and b) x_2 coordinate at mid chord for an initially flat, constant tension membrane wing, $\Pi_1 = 0$, $\Pi_2 = 2$, and $\varepsilon = 0$; 100 grid points were used along the wing chord.

unpretensioned elastic membrane wing of Fig. 8 has very little initial resistance to deformation, and consequently, a substantial amount of camber exists in the equilibrium configuration near 0 deg angle of attack. Conversely, the pretensioned membrane wing of Fig. 9 has adequate stiffness in its initially flat unstrained configuration to postpone the development of camber until higher angles of attack are reached. For the constant tension wing of Fig. 9 the lift curve closely mimics the development of camber with angle attack as was the case with the elastic wing of Fig. 8.

Inextensible Membrane Case

Finally, the limiting case of a flexible but inextensible membrane wing with excess length is investigated. The nondimensional parameters are $\varepsilon = 0.017$, $\Pi_1 = 46$, and $\Pi_2 = 0$. The excess length and aeroelastic parameters were chosen to reproduce a portion of the experimental data reported by Newman and Low.[15] Experience has shown that for this excess length any further increase in Π_1 will not substantially affect the aeroelastic solution. Consequently, the present computations are for a membrane wing that may be considered essentially inextensible. Because of the assumption of steady laminar flow the numerical computations were limited to Reynolds numbers below 4×10^3, whereas the Reynolds number reported by Newman and Low[15] was 1.2×10^5, which is in the turbulent flow regime.

The effect of grid refinement on the computed streamlines for the inextensible membrane wing at a Reynolds number of 4×10^3 and 0 deg angle of attack is shown in Fig. 10. As may be seen in the figure, a large recirculation region appears on the lower surface of the membrane as the grid is refined. The integrated aerodynamic properties and the nominal membrane tension are given in Table 3 for the grid refinement sequence of Fig. 10. Even for the highest grid resolution shown the tabulated values of lift and tension are not yet grid independent. Of course, the membrane lift and tension

Table 3 Effect of grid refinement on computed aeroelastic properties for an inextensible membrane wing at $\alpha = 0$ deg, $\Pi_1 = 46$, $\Pi_2 = 0$, $\varepsilon = 0.017$, and $Rn = 4 \times 10^3$

Grid	Points on c	C_L	C_D	C_M	C_T	max x_2
261 × 101	100	0.378	0.0716	0.152	0.893	0.0836
361 × 121	200	0.342	0.0689	0.144	0.823	0.0835
461 × 141	300	0.317	0.0685	0.139	0.773	0.0835
561 × 141	400	0.300	0.0702	0.136	0.741	0.0834

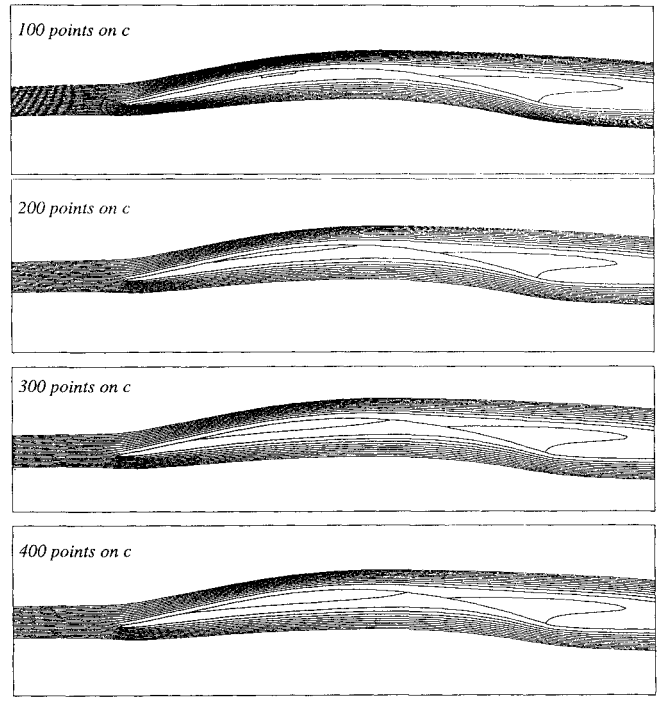

Fig. 10 Effect of grid refinement on stream function contours for an inextensible membrane wing at $\alpha = 0$ deg, $\Pi_1 = 46$, $\Pi_2 = 0$, $\varepsilon = 0.017$, and $Rn = 4 \times 10^3$.

will follow the same trend as the grid is refined as required by equilibrium.

Figure 11 contrasts the viscous flow based aeroelastic solution with a potential flow based aeroelastic solution for the inextensible membrane wing. Although the equilibrium membrane profiles are similar, as shown in Fig. 11a, the surface pressures, shown in Fig. 11b, are dramatically different. In particular, near the leading edge the pressure jumps across the membrane Δp predicted by the two flow models are of different sign. The negative Δp computed by the viscous flow model implies an inflection point in the equilibrium membrane profile that, upon close inspection, may be seen in the figure. In contrast, the potential-based model predicts a flow pattern and a membrane profile that is completely symmetric about the midchord. It may be concluded that, for this set of dimensionless parameters, a potential flow based membrane wing theory essentially fails.

Figure 12a compares the computed, laminar flow equilibrium lift coefficient at Reynolds numbers of 2×10^3 and 4×10^3 with the experimental data of Newman and Low.[15] The disagreement between the computational and experimental results is largely due to the assumption of laminar flow in the present computation.

The decrease in lift with increasing Reynolds number shown in Fig. 12a is contrary to the trend observed in the previous computations on membrane wings. This trend may be explained by observing that the separation point x_1^{sp} (defined as the point of vanishing shear stress) moves forward along the membrane as the Reynolds number is increased as shown in Fig. 12b. The presence of turbulent mixing in the boundary layer would undoubtedly postpone flow separation and lead to higher lift coefficients consistent with the experimental data. Also shown in Fig. 12a is the computed equilibrium lift using a potential based membrane wing theory. The potential flow based aeroelastic solution is seen to considerably overestimate the lift on

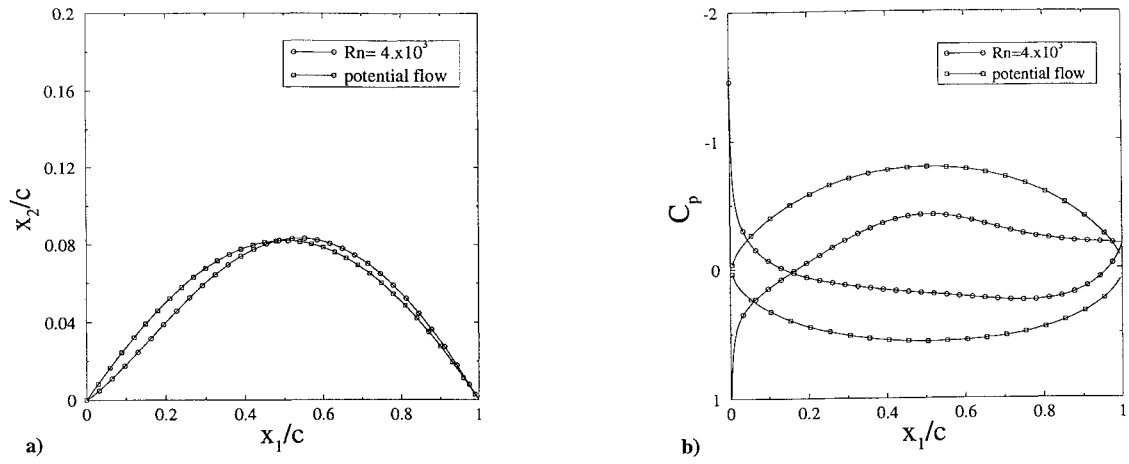

Fig. 11 Comparison of a) potential and viscous flow based membrane configurations and b) surface pressures for an inextensible membrane wing with excess length; $\Pi_1 = 46$, $\Pi_2 = 0$, $\varepsilon = 0.017$, and $\alpha = 0$ deg; 400 grid points were used along the wing chord.

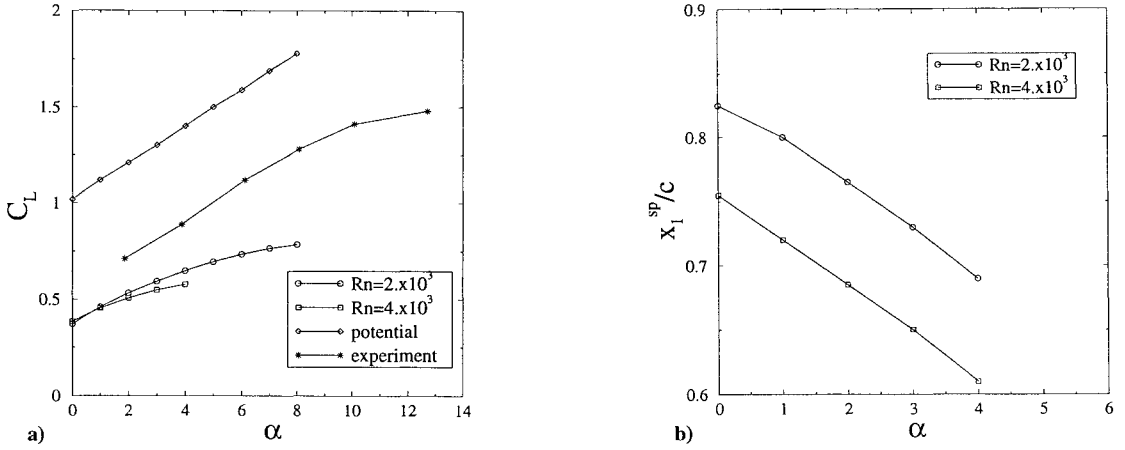

Fig. 12 Comparison of a) lift coefficient with experimental data and b) separation point for an inextensible membrane wing with excess length; $\Pi_1 = 46$, $\Pi_2 = 0$, and $\varepsilon = 0.017$; 100 grid points were used along the wing chord.

the membrane wing when compared with the experimental results. Conversely, the viscous, laminar flow based model considerably underestimates the lift reported by Newman and Low.[15] The extension of the model to the turbulent flow regime is currently under way.

Summary

In the present work a numerical model simulating the aeroelastic characteristics of a flexible two-dimensional membrane wing in a viscous fluid has been presented. The use of the Navier–Stokes equations as the fluid dynamic model in the present model is a substantial departure from previous work on membrane wing aerodynamics that has, almost universally, adopted a potential based description of the flowfield.

The two-dimensional aeroelastic boundary value problem was nondimensionalized, and a set of five basic dimensionless parameters that govern the solution of the problem was derived. A numerical procedure was then developed for the solution of the coupled aeroelastic problem. The role of viscosity in membrane wing aerodynamics was investigated using the numerical model for steady flows. These investigations were facilitated by distinguishing three classes of problems that are associated with corresponding limiting cases of the dimensionless parameter set. The aerodynamic characteristics of membrane wings at Reynolds numbers between 2×10^3 and 10^4 were shown to be substantially different from those predicted by a potential based membrane wing theory.

Acknowledgments

The authors would like to acknowledge General Electric Company for partially supporting the present work and also to thank Eglin Air Force Base for the use of their Cray Y-MP computer.

References

[1]Voelz, K., "Profil und Luftriebeines Segels," *ZAMM*, Vol. 30, 1950, pp. 301–317.

[2]Thwaites, B., "Aerodynamic Theory of Sails," *Proceedings of the Royal Society of London*, Vol. 261, 1961, pp. 402–442.

[3]Nielsen, J. N., "Theory of Flexible Aerodynamic Surfaces," *Journal of Applied Mechanics*, Vol. 30, 1963, pp. 435–442.

[4]Chambers, L. I., "A Variational Formulation of the Thwaites Sail Equation," *Quarterly Journal of Mechanics and Applied Mathematics*, Vol. 19, 1966, pp. 221–231.

[5]Newman, B. G., "Aerodynamic Theory for Membranes and Sails," *Progress in Aerospace Sciences*, Vol. 24, 1987, pp. 1–27.

[6]Greenhalgh, S., Curtiss, H. C., and Smith, B., "Aerodynamic Properties of Two-Dimensional Inextensible Flexible Airfoils," *AIAA Journal*, Vol. 22, 1984, pp. 865–870.

[7]Vanden-Broeck, J. M., and Keller, J. B., "Shape of a Sail in a Flow," *Physics of Fluids*, Vol. 24, 1981, pp. 552–553.

[8]Sugimoto, T., and Sato, J., "Aerodynamic Characteristics of Two-Dimensional Membrane Airfoils," *Japan Society for Aeronautical and Space Sciences Journal*, Vol. 36, 1988, pp. 36–43.

[9]Vanden-Broeck, J. M., "Nonlinear Two-Dimensional Sail Theory," *Physics of Fluids*, Vol. 25, 1982, pp. 420–423.

[10]Murai, H., and Maruyama, S., "Theoretical Investigation of the Aerodynamics of Double Membrane Sailwing Airfoil Sections," *Journal of Aircraft*, Vol. 17, 1980, pp. 294–299.

[11]Jackson, P. S., "A Simple Model for Elastic Two-Dimensional Elastic Sails," *AIAA Journal*, Vol. 21, 1983, pp. 153–155.

[12]Sneyd, A. D., "Aerodynamic Coefficients and Longitudinal Stability of Sail Airfoils," *Journal of Fluid Mechanics*, Vol. 149, 1984, pp. 127–146.

[13]Murata, S., and Tanaka, S., "Aerodynamic Characteristics of a Two-Dimensional Porous Sail," *Journal of Fluid Mechanics*, Vol. 206, 1989, pp. 463–475.

[14]de Matteis, G., and de Socio, L., "Nonlinear Aerodynamics of a Two-Dimensional Membrane Airfoil with Separation," *AIAA Journal*, Vol. 23, 1986, pp. 831–836.

[15]Newman, B. G., and Low, H. T., "Two-Dimensional Impervious Sails: Experimental Results Compared with Theory," *Journal of Fluid Mechanics*, Vol. 144, 1984, pp. 445–462.

[16]Jackson, P. S., and Fiddes, S., "Two-Dimensional Viscous Flow Past Flexible Sail Sections Close to Ideal Incidence" (unpublished paper).

[17]Shyy, W., *Computational Modeling for Fluid Flow and Interfacial Transport*, Elsevier, Amsterdam, The Netherlands, 1994.

[18]Seide, P., "Large Deflections of Rectangular Membranes Under Uniform Pressure," *International Journal of Nonlinear Mechanics*, Vol. 12, 1977, pp. 397–406.

[19]Patankar, S. V., and Spalding, D. B., "A Calculation Procedure for Heat, Mass and Momentum Transfer in Three-Dimensional Parabolic Flows," *International Journal of Heat and Mass Transfer*, Vol. 15, 1972, pp. 1787–1806.

[20]Patankar, S. V., *Numerical Heat Transfer and Fluid Flow*, Hemisphere, Washington, DC, 1980.

[21]Braaten, M., and Shyy, W., "A study of Recirculating Flow Computation Using Body-Fitted Coordinates: Consistency Aspects and Mesh Skewness," *Numerical Heat Transfer*, Vol. 9, 1986, pp. 559–574.

[22]Shyy, W., Thakur, S., and Wright, J., "Second-Order Upwind and Central Difference Schemes for Recirculating Flow Computation," *AIAA Journal*, Vol. 30, 1992, pp. 923–932.

[23]Boschitsch, A. H., and Quackenbush, T. R., "High Accuracy Computation of Fluid-Structure Interaction in Transonic Cascades," AIAA Paper 93-0485, Jan. 1993.

[24]James, R. M., "On the Remarkable Accuracy of the Vortex Lattice Method," *Computer Methods in Applied Mechanics and Engineering*, Vol. 1, 1972, pp. 55–79.

[25]Katz, J., and Plotkin, A., *Low Speed Aerodynamics*, McGraw–Hill, New York, 1991.